Effective Connectivity of Cortical Sensorimotor Networks During Finger Movement Tasks: A Simultaneous fNIRS, fMRI, EEG Study

A. R. Anwar[1,2] · M. Muthalib[3,4] · S. Perrey[3] · A. Galka[5] · O. Granert[6] ·
S. Wolff[7] · U. Heute[1] · G. Deuschl[6] · J. Raethjen[6] · Muthuraman Muthuraman[6,8]

Abstract Recently, interest has been growing to understand the underlying dynamic directional relationship between simultaneously activated regions of the brain during motor task performance. Such directionality analysis (or effective connectivity analysis), based on non-invasive electrophysiological (electroencephalography— EEG) and hemodynamic (functional near infrared spectroscopy—fNIRS; and functional magnetic resonance imaging—fMRI) neuroimaging modalities can provide an estimate of the motor task-related information flow from one brain region to another. Since EEG, fNIRS and fMRI modalities achieve different spatial and temporal

A. R. Anwar and M. Muthalib have contributed equally to this work.

✉ Muthuraman Muthuraman
  m.muthuraman@neurologie.uni-kiel.de

[1] Faculty of Digital Signal Processing and System Theory, University of Kiel, Kiel, Germany

[2] Biomedical Engineering Department, UET Lahore (KSK), Lahore, Pakistan

[3] EuroMov, University of Montpellier, Montpellier, France

[4] Movement Neuroscience, Queensland University of Technology, Brisbane, Australia

[5] Department of Neuropediatrics, University of Kiel, Kiel, Germany

[6] Department of Neurology, University of Kiel, Kiel, Germany

[7] Department of Neuroradiology, University of Kiel, Kiel, Germany

[8] Department of Neurology, Johannes Gutenberg University, Mainz, Germany

resolutions of motor-task related activation in the brain, the aim of this study was to determine the effective connectivity of cortico-cortical sensorimotor networks during finger movement tasks measured by each neuroimaging modality. Nine healthy subjects performed right hand finger movement tasks of different complexity (simple finger tapping-FT, simple finger sequence-SFS, and complex finger sequence-CFS). We focused our observations on three cortical regions of interest (ROIs), namely the contralateral sensorimotor cortex (SMC), the contralateral premotor cortex (PMC) and the contralateral dorsolateral prefrontal cortex (DLPFC). We estimated the effective connectivity between these ROIs using conditional Granger causality (GC) analysis determined from the time series signals measured by fMRI (blood oxygenation level-dependent-BOLD), fNIRS (oxygenated-O_2Hb and deoxygenated-HHb hemoglobin), and EEG (scalp and source level analysis) neuroimaging modalities. The effective connectivity analysis showed significant bi-directional information flow between the SMC, PMC, and DLPFC as determined by the EEG (scalp and source), fMRI (BOLD) and fNIRS (O_2Hb and HHb) modalities for all three motor tasks. However the source level EEG GC values were significantly greater than the other modalities. In addition, only the source level EEG showed a significantly greater forward than backward information flow between the ROIs. This simultaneous fMRI, fNIRS and EEG study has shown through independent GC analysis of the respective time series that a bi-directional effective connectivity occurs within a cortico-cortical sensorimotor network (SMC, PMC and DLPFC) during finger movement tasks.

Introduction

In recent years combinations of different electrophysiological and hemodynamic neuroimaging modalities have emerged as tools for non-invasively measuring functional brain activation and connectivity of cortical networks during motor and cognitive tasks in healthy and clinical populations (Biswal et al. 1995; Ferrari and Quaresima 2012; Shibasaki 2008; Xiong et al. 1999). Electrophysiological measurement techniques such as electroencephalography (EEG) and magnetoencephalography (MEG) measure functional brain activity directly by detecting the variations of electrical (Blinowska and Malinowski 1991; Leuchter et al. 1992; Niedermeyer and da Silva 2005; Schelter et al. 2006) or magnetic (Andres and Gerloff 1999; Cohen 1968; Nikouline et al. 2001; Schnitzler and Gross 2005) fields, respectively. On the other hand, hemodynamic measurement techniques such as functional magnetic resonance imaging (fMRI) and functional near infrared spectroscopy (fNIRS) measure functional brain activity indirectly via changes in the fMRI blood oxygenation level-dependent (BOLD) signal, or via changes in fNIRS oxygenated (O_2Hb) and deoxygenated (HHb) hemoglobin concentrations. These hemodynamic measurements are related to an increase in regional cerebral blood flow subsequent to increased neuronal activity (i.e., a consequence of neurovascular coupling) (Attwell and Iadecola 2002).

The functional network of cortical regions of interest (ROIs) involved in rhythmic and sequential finger movements in healthy subjects has been analyzed using EEG (Muthuraman et al. 2012), MEG (Pollok et al. 2004), fMRI (Nedelko et al. 2010; Wu and Hallett 2005) and fNIRS (Leff et al. 2011) separately, and the SMC, PMC and DLPFC are three core regions of the cortical sensorimotor network for movement control (Witt et al. 2008). Our previous case study (Muthalib et al. 2013) has shown the feasibility of simultaneously measuring contralateral SMC activation by EEG, fMRI and fNIRS measurements during right hand finger movement tasks and also showed that a good correlation between the time series signals of the three neuroimaging modalities can be obtained. Although detecting activation of a specific region of the brain during task performance can provide information on how for example motor task speed influences the SMC activation, it does not provide information on how different ROIs in a sensorimotor network communicate with each other during performance of the motor task. Functional connectivity of cortical networks refers to the task-related interactions between spatially different cortical ROIs, which can be measured by covariance analyses of time series signals extracted from both electrophysiological and hemodynamic neuroimaging techniques (Büchel and Friston 1997; Engel et al. 2001; Shibasaki 2008). Additionally another robust way of attesting functional connectivity in the human cortical motor system could be cortical–cortical evoked potential (Matsumoto et al. 2007). However, functional connectivity does not explain the direction of information flow between the cortical ROIs; it only gives the correlation between them. Recent advances in neuroimaging signal analysis have enabled researchers to estimate directional coupling of information flow between cortical ROIs, which is referred to as *effective connectivity* or *functional causality* (Ewald et al. 2012; Friston et al. 2003). Various algorithms have been proposed to measure the effective connectivity between different cortical ROIs and applied to both hemodynamic-based (fMRI, fNIRS) and electrophysiology-based (EEG) modalities (Baccalá and Sameshima 2001; Baccalá et al. 2007; Kaminski and Blinowska 1991; Korzeniewska et al. 2003). The conditional Granger causality (GC) analysis is one such method which can determine the effective connectivity of functional networks by analysis of time series signals recorded from different ROIs in the brain (Granger 1969). Calculation of GC is built on multivariate autoregressive (MVAR) modeling, and the idea behind GC is based on the fact that one time series is useful in predicting another time series. The network of effective connectivity interactions between cortical ROIs namely SMC, PMC, DLPFC during a finger tapping task in healthy subjects has been presented in earlier studies using MEG or EEG source analysis (Muthuraman et al. 2012; Pollok et al. 2004, 2006). A number of previous studies have successfully applied GC analysis to fMRI data during motor and cognitive tasks (Abler et al. 2006; Anwar et al. 2012; Hwang et al. 2010; Wen et al. 2012). The GC analysis has also been applied to fNIRS data to determine the effective connectivity between cortical ROIs in animal (Im et al. 2010; Yuan 2013) and human (Bajaj et al. 2014) experiments. In the above-mentioned studies, using one or two neuroimaging modalities simultaneously have shown bi-directional or uni-directional information flow patterns between the SMC, PMC and DLPFC ROIs. However, to the best of our knowledge no previous study has utilized fNIRS, EEG and fMRI neuroimaging approaches simultaneously to determine the effective connectivity of the same cortico-cortical sensorimotor networks (SMC, PMC, and DLPFC) during different finger movement tasks. Since EEG, fNIRS and fMRI modalities achieve different spatial and temporal resolutions of motor-task related activation in the brain; we surmise that an integrated multimodal neuroimaging approach may also be able to provide a unique perspective to understand the properties of the complex networks of the human brain during motor tasks.

Therefore, the present study aimed at applying GC analysis to the EEG, fMRI and fNIRS time series signals in order to determine the effective connectivity of the contralateral cortico-cortical sensorimotor network (SMC, PMC, and DLPFC) during simple and complex finger movement tasks of the right hand. We expect that the cortico-cortical directional coupling determined independently by the three-neuroimaging modalities (fMRI, fNIRS and EEG) provide bi-directional information flow pattern between the contralateral SMC, PMC and DLPFC ROIs during simple and complex finger movement tasks.

Materials and methods

Subjects

Nine healthy subjects (mean age 27 years, range 21–38 years, five female) volunteered to participate in the study. All subjects were right handed as determined by the Edinburgh handedness questionnaire (Oldfield 1971). The study conformed to the recommendations of the local Human Research Ethics Committee in accordance with the Declaration of Helsinki. All participants provided written consent prior to participating in the study.

Finger Movement Tasks

The finger movement tasks included simple finger tapping (FT), simple finger sequence (SFS) and complex finger sequence (CFS) tasks. Tapping the index finger in a rhythmic fashion to have at least 2–5 finger taps per second was the FT task. Sequential tapping of the index, middle, ring and fourth finger against the thumb was the SFS task; while the CFS task was performed by sequential tapping of the index, ring, middle and fourth finger against the thumb. A block design was used in which subjects were asked to perform the finger movement tasks for 30 s followed by 30 s rest. Hence ten complete (task-rest) blocks were obtained for each finger movement task resulting in 10 min per task. A 2 min rest period separated each movement task. In order to help subjects with the timing and sequence of the finger movements, a visual stimulus was presented on a screen in the fMRI scanner (see Sect. 2.2.1. for details) using E-prime software (Psychology Software Tools, Inc., Sharpsburg, USA) (Kikuchi et al. 2012). The rhythmic finger movement rates were checked from each subject by inspecting the electromyography (EMG) activity (see Sect. 2.2.2 for details) online to have at least 2–5 finger taps per second.

Simultaneous Neuroimaging Measurements

fMRI

BOLD-sensitive MRI was performed with a 3-Tesla MR scanner (Philips Achieva, Philips, Best, The Netherlands) and a standard 8-channel SENSE head coil. T1 MRI images were acquired with a standard MP-RAGE sequence with an isotropic voxel resolution of 1 mm. A single-shot T2*-weighted, gradient-echo planar imaging sequence was used for fMRI (TR = 2500 ms, TE = 45 ms, 32 slices, 64 × 64 matrix, slice thickness = 3.5 mm, FOV = 200 mm, flip angle = 90°). The sampling rate was 0.4 Hz, such that 240 brain volume images were acquired during 10 min of recording for each motor task (Anwar et al. 2012).

Preprocessing of fMRI scans and time series extraction were performed using (MATLAB R2013a, 8.1.0.604, The Mathworks Inc., MA, USA software with SPM8 http://www.fil.ion.ucl.ac.uk/spm) toolbox. Realignment was first performed to remove movement related artifacts in fMRI time series. In order to realign, the first image from the recording was specified as the reference image and all subsequent images were realigned to it. In addition to realignment, scans were normalized to align all the subjects' specific MR sequences into the standard Montreal Neurological Institute (MNI) space. The scans were smoothed by convolving them with a Gaussian kernel of fixed width (full width half maximum 8 × 8 × 8 mm) to suppress noise and effects due to differences in functional and gyral anatomy.

For the statistical analysis of the fMRI data a general linear model (GLM) was specified to model the BOLD signal during the fMRI session. Tasks were modeled by a block design with a task condition that has 10 blocks of a 30 s activity alternated by 30 s of rest. The localization of task related activity was then detected by specifying a positive t-contrast on the task condition. To avoid inordinate false positives findings due to multiple statistical comparisons in each voxel, we applied the FWE correction with p value threshold of 0.05 to the statistical t-map and in addition a cluster size based criterion that at least 5 contiguous voxels must be activated. Based on these filtered statistical maps, time series were extracted from the three contralateral ROIs: SMC, PMC and DLPFC (see Table 1 for the corresponding MNI co-ordinates). A sphere with a radius of 3 mm was extracted around the center voxel. The radius of 3 mm was chosen to restrict the extracted signal clearly to the selected ROIs; especially to distinguish the signals between the proximate SMC and PMC ROIs. We considered that the effective fMRI (BOLD) time series extracted from this 3 mm sphere will yield the neuronal

Table 1 Individual subject MNI co-ordinates of the maximum activated voxel (fMRI) and maximum coherent voxel (source level EEG) in the sensorimotor cortex (SMC), premotor cortex (PMC) and dorsolateral prefrontal cortex (DLPFC) regions of interest for the three finger movement tasks (finger tapping-FT, simple finger sequence-SFS, complex finger sequence-CFS)

Subject	Task	fMRI									EEG									Euclidean distance between EEG and IMRI (mm)		
		SMC			PMC			DLPFC			SMC			PMC			DLFC					
		X	Y	Z	X	Y	Z	X	Y	Z	X	Y	Z	X	Y	Z	X	Y	Z			
1	FT	−29	−26	54	−23	8	17	−30	16	35	−28	−25	55	−23	6	16	−30	17	33	1.73	2.24	2.24
	SFS	−30	−25	57	−25	8	17	−30	17	34	−29	−26	55	−24	7	17	−31	16	33	1.00	1.41	2.24
	CFS	−28	−25	56	−24	7	17	−27	18	36	−32	−24	54	−24	8	16	−28	18	34	3.00	1.41	3.00
2	FT	−31	−27	56	−24	6	17	−27	17	33	−29	−22	54	−25	7	16	−30	17	33	3.00	2.45	2.24
	SFS	−27	−23	54	−24	8	17	−28	16	32	−30	−23	57	−24	8	17	−28	17	32	2.36	1.00	2.74
	CFS	−28	−26	57	−23	6	16	−29	17	32	−28	−27	57	−25	8	16	−30	18	35	3.00	2.24	2.00
3	FT	−27	−26	56	−24	6	15	−30	18	32	−31	−23	56	−25	7	17	−30	18	33	3.00	2.24	2.83
	SFS	−27	−24	55	−25	8	18	−29	17	34	−28	−26	54	−24	7	18	−27	17	34	1.00	1.73	3.00
	CFS	−31	−25	56	−24	6	16	−30	18	34	−30	−25	55	−24	6	17	−28	18	35	1.73	2.24	2.83
4	FT	−30	−22	55	−24	8	15	−30	17	33	−30	−27	55	−23	9	16	28	17	33	1.73	1.41	3.00
	SFS	−29	−22	54	−23	8	17	−31	19	35	−31	−22	56	−23	7	17	−30	19	35	2.90	1.00	3.00
	CFS	−32	−25	55	−24	8	18	−29	17	35	−32	−24	54	−24	6	15	−30	18	34	3.00	3.00	2.24
5	FT	−27	−26	54		6	17	−28	18	35	−30	−23	54	−24	7	18	−28	17	35	3.00	1.73	2.24
	SFS	−29	−27	55	−24	8	16	−27	17	36	−28	−27	55	−24	7	18	−30	18	35	1.73	1.73	2.00
	CFS	−29	−23	55	−24	8	16	−29	17	36	−28	−22	56	−25	7	17	−30	18	34	2.58	2.24	2.24
6	FT	−31	−25	55	−24	9	18	−30	16	33	−28	−26	56	−24	7	16	−27	18	32	2.24	1.73	2.69
	SFS	−31	−24	54	−25	8	15	−29	18	33	−31	−26	56	−24	9	17	−29	19	33	2.83	1.41	2.74
	CFS	−28	−22	57	−23	8	18	−27	18	35	−28	−26	55	−25	9	15	−29	17	34	1.41	3.00	1.73
7	FT	−29	−24	57	−25	7	18	−28	18	32	−31	−22	56	−25	6	16	−31	17	33	2.90	3.00	2.45
	SFS	−29	−23	55	−25	7	17	−28	17	34	−28	−24	55	−24	8	16	−27	16	33	2.45	1.41	2.61
	CFS	−30	−26	55	−25	8	16	−28	18	34	−32	−23	56	−23	7	15	−29	19	35	2.69	2.24	2.16
8	FT	−31	−24	55	−23	6	16	−29	18	35	−29	−26	55	−23	7	16	−29	18	34	1.00	1.41	2.45
	SFS	−31	−25	57	−24	6	16	−29	18	34	−28	−24	56	−25	8	16	−29	17	36	3.00	2.24	1.73
	CFS	−28	−23	55	−24	7	16	−29	18	34	−28	−27	55	−23	9	15	−30	18	34	1.73	2.24	2.24
9	FT	−30	−25	54	−24		15	−31	19	35	−30	−23	55	−24	7	17	−28	18	35	2.32	1.41	2.83
	SFS	−30	−23	56	−23	8	17	−29	17	35	−29	−23	56	−23	9	16	−30	18	34	2.61	1.41	2.24
	CFS	−28	−25	55	−24	8	16	−31	18	34	−29	−23	56	−25	7	17	−29	18	35	2.61	2.24	2.24

The last column shows the mean Euclidean distance between the EEG and fMRI MNI co-ordinates

activity which is the source of cortical activation in the respective ROIs (Zhang et al. 2010). In order to check the selection of the sphere radius, fMRI data was parcelled using an anatomical template called Automated Anatomic Labelling (AAL) atlas and then the fMRI-BOLD signals were extracted from the three ROIS (SMC, PMC and DLPFC) and the GC analyses were repeated to see the effective connectivity.

EEG

EEG was recorded with a MR-compatible high-resolution 256-channel recording system (Electrical Geodesics Inc, OR, USA), using CZ as reference. The surface EMG activity was recorded from the right hand forearm flexors and extensors using pre-gelled AgCI electrodes (Brain Products Co., Munich, Germany). The ECG was recorded with two standard AgCI bipolar electrodes placed on the left anterior axillary line in the 5th intercostal space and the 2nd intercostal space right of the sternum. The EEG and EMG signals were simultaneously sampled at 1000 Hz, stored on a PC and analyzed offline using MATLAB (Matlab R2013a, 8.1.0.604, The Mathworks Inc., MA, USA). The EEG coherence and the source analyses were performed with the open source toolbox fieldtrip (Oostenveld et al. 2010). Data were transmitted from the amplifier, which was placed directly in front of the head coil inside the MRI scanner room and connected to a PC located outside the scanner room, via a fiber optic cable. The fMRI scanner 10 MHz clock signal was used for synchronizing the fMRI (BOLD) measurements with the EEG amplifier.

The EEG and EMG signals were first band-pass filtered (EEG 0.05–200 Hz; EMG 30–200 Hz). EMG was full-wave rectified; the combination of band-pass filtering and rectification is the common demodulation procedure for EMG (Journee 2007). Online correction of EEG gradient artifacts based on the *average artifact subtraction* algorithm was performed using the EGI software (Electrical Geodesics Inc., OR, USA), enabling visual inspection of the EEG with a sliding average of 50 TRs (Allen et al. 1998, 2000). In order to eliminate the ballistocardiogram artifact, a very similar subtraction procedure was used (Michels et al. 2013). In the elimination procedure the artifact window was aligned on QRS complexes detected in the ECG traces and the templates were composed from 10 consecutive pulse intervals and individually estimated time delay based on the global field power distribution. The residual gradient artifacts, eye blinks were removed using a regression-based method (Gratton et al. 1983).

EEG-Scalp Level The EEG-data were re-referenced to the common average reference and was used for all the subsequent analyses. In this step the average of all the 256 EEG electrodes were estimated and the average was then used as the re-reference for all the EEG electrodes. We then calculated the periodogram (Halliday et al. 1995) of the EEG power spectra and the cross spectrum of EEG and EMG for each of the 1-s segments independently using a Hanning window. These periodograms were then averaged over all the segments to get a reliable spectral and cross spectral estimate with a frequency resolution of 1 Hz. EEG-EMG coherence measures the linear time-invariant relationship between EEG and EMG signals; it is calculated as the ratio of the squared magnitude of the cross spectrum to the product of the power spectra. The confidence limit which indicates the significance of EEG-EMG coherence at a particular frequency is calculated by $1 - (1 - \chi^{1/M-1})$ where M is the number of disjoint segments used for the estimation, and χ is set to 0.99, so that the confidence limit results as $1 - 0.01^{1/M-1}$ (Govindan et al. 2005; Halliday et al. 1995). Values of EEG-EMG coherence above this confidence limit $(1 - 0.01^{1/M-1})$ indicates a significant correlation between the two time series, while values below this limit indicate absence of correlation. The C3, FC3 and F3 electrodes were used to represent the scalp level EEG channels corresponding to the SMC, PMC, and DLPFC ROIs respectively (see Fig. 1).

EEG-Source Level In order to locate the origin (i.e., the source) of neuronal activity seen on the scalp EEG signals during the finger movement tasks, two problems needed to be solved, namely the forward and the inverse problem. The forward problem is the computation of scalp potentials for a set of neural current sources in the brain, which is

usually solved by estimating the so-called lead field matrix with specified models for the brain. The lead field matrix was constructed using the realistic volume conductor model (Fuchs et al. 2002), using a boundary element method consisting of three non-intersecting, closed surface separating compartments of isotropic and homogenous layers with conductivity values: 0.33, 0.0042, and 0.33 S/m for the brain, skull and scalp, respectively (Fuchs et al. 2002). Meshes of triangles modeled the three surfaces. These surfaces were obtained from each subject's anatomical T1 MRI by setting different threshold values for each layer such that they did not overlap.

The inverse problem is the quantitative estimation of the neural sources underlying the observed neural activity. The source analysis used here was the dynamic imaging of coherent sources (DICS) method based on the beam forming approach (Gross et al. 2001; Sekihara and Scholz 1996). For visualizing the EEG power and coherence in the brain at a given frequency range, a linear transformation was used based on a constrained optimization problem which acts as a spatial filter (Van Veen et al. 2002). By taking the EMG as the reference signal, the brain region representing the strongest coherence in a specific frequency band was identified. The criteria used to identify more coherent areas were selected by a within-subject surrogate analysis, in order to define the significance level individually for each subject. The surrogates were estimated by Monte Carlo random permutations of 100 times of 1-s segments within each subject. The p value for each of these 100 random permutations was estimated and then the mean distribution of the p value was taken as the significance level in each subject. This was the limit for considering areas in the brain or activated voxels as noise for the next run of source analysis and subsequently identifying other areas in the brain for the same EMG reference signal. In order to create tomography maps, a spatial filter was applied to a large number of voxels covering the entire brain using a voxel size of 5 mm. The individual maps of the strongest EEG-EMG coherence were spatially normalized, averaged and displayed on a standard MNI template brain in SPM8. The same procedure for the analysis was followed for each subject separately, followed by a grand average across all the subjects. Once coherent areas were identified, their activity was extracted from the surface EEG signals. In a subsequent analysis, all the activated voxels within the source signals were subjected to a pooled estimate. This was done by pooling the second order spectra using a weighting scheme and estimating the pooled estimate as previously described (Amjad et al. 1997; Rosenberg et al. 1989). For each of the subjects, the pooled source signals from each of these sources were taken and then the dynamical coherence (DCA) was

Fig. 1 256 channel EEG electrode layout on a realistic head model skin from the sagittal (**a**) and coronal (**b**) viewpoint. The scalp EEG electrodes (C3, FC3, F3) and fNIRS measurement locations (area between transmitter-T and Receiver-R) corresponding to the SMC, PMC, and DLPFC regions of interest
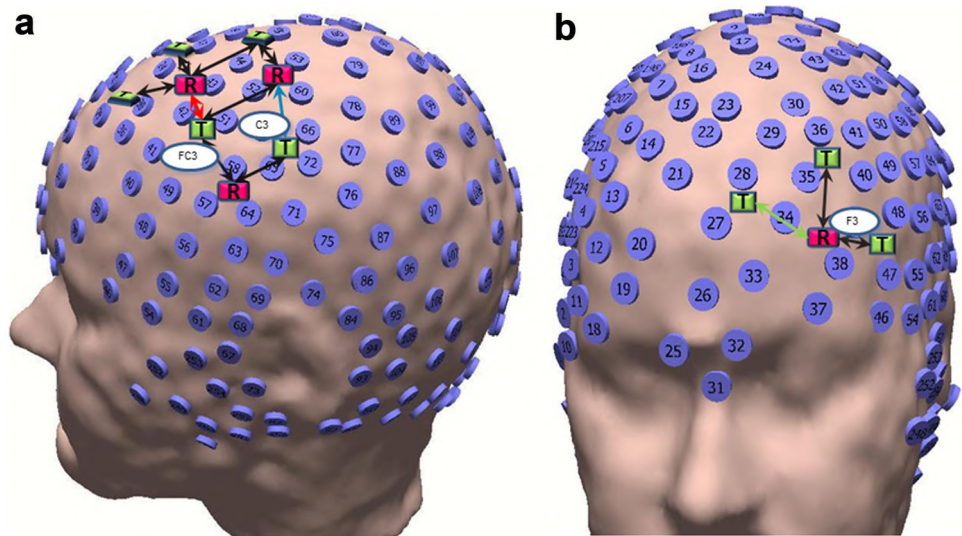
estimated with the EMG to attain the DCA source signal vector at the individual finger movement frequency.

In all the subjects the source analysis was applied on the basis of the EEG-EMG coherence peak frequency (2–5 Hz), and the sources which were active in the analyzed frequency were identified. The sources were restricted to the three contralateral ROIs (SMC, PMC and DLPFC) in order to perform a direct comparison with the fMRI and fNIRS neuroimaging modalities. The voxel with the maximum coherence that was coherent between EEG and EMG from all the activated voxels in these three ROIs were identified and then the time series was extracted for further analysis. In order to test that the identified voxel was the most appropriate one from the EEG source analysis, the Euclidean distance between the maximum coherent voxel from the EEG and the maximum activated voxel based on the t-value from the fMRI for the three ROIs and finger movement tasks was calculated (see Table 1). The same procedure was done to determine the mean Euclidean distance between the three scalp EEG electrodes and the maximum activated voxel in the fMRI for all the three tasks and the three ROIs (see Table 1).

fNIRS

An MR-compatible continuous-wave multi-channel fNIRS system (Oxymon Mk III, Artinis Medical Systems, The Netherlands) was used to measure the concentration changes of O_2Hb and HHb in the cortical microcirculation blood vessels by means of the characteristic absorption spectra of hemoglobin in the near-infrared range. Two wavelengths (856 and 781 nm) per channel were used at a sampling rate of 10 Hz. Five detector (avalanche photo diode) and 11 transmitter (pulsed laser diode) probes were

placed in the EEG cap using specially designed holders, to obtain 15 channels (each represented by a Transmitter-Detector combination) with the distance between each transmitter and detector set to 3–3.5 cm (see Fig. 1). Fiducial markers were placed between each transmitter and detector pair so that the position of the fNIRS channel could be located in the T1-MR images of each subject. After the fNIRS probes were placed in the EEG cap and secured in place by a cloth, subjects were placed inside the MRI scanner. MR-compatible fNIRS optical fibers of ~ 10 m length were used to connect to the fNIRS system located outside the MRI room. The fMRI scanner 10 MHz clock signal was also synchronized with the fNIRS system.

The fNIRS channels were first located on each subject's T1-MRI using the fiducial markers. The selection of the fNIRS channels to represent the three contralateral ROIs (SMC, PMC, and DLPFC) were based on the fNIRS channels that satisfied the condition that it lay anatomically in the region above the fMRI (BOLD) maximum activated voxel and the fiducial markers were used as the reference. Then the time series of one fNIRS channel from each of the three contralateral ROIs (SMC, PMC, and DLPFC) was selected for each subject based on the fNIRS channel that had the best functional correlation with the fMRI time series (Muthalib et al. 2013; see supplementary Table 1 for group level functional correlations between the fNIRS, fMRI and EEG modalities).

Effective Connectivity Analysis Using Granger Causality

The steps for the GC analysis for the fMRI, EEG and fNIRS neuroimaging modalities are illustrated as a flow chart in supplementary Fig. 1. The scalp level EEG GC

analysis was performed on the time series extracted from the C3, FC3 and F3 electrodes corresponding to the contralateral SMC, PMC, and DLPFC ROIs respectively (see Fig. 1). The source level EEG GC analysis was performed on the time series extracted from the maximal coherent voxel in the contralateral SMC, PMC and DLPFC ROIs (see Fig. 2). The fMRI (BOLD) time series signals were extracted from the peak activated voxel in the contralateral SMC, PMC and DLPFC ROIs (see Fig. 3). The fNIRS (O_2Hb and HHb) GC analysis was performed on the time series extracted from three channels corresponding to the contralateral SMC, PMC, and DLPFC ROIs respectively. For the fMRI and fNIRS, the mean time series was removed from the time series in order to have a zero mean prior to the GC analysis (Seth et al. 2013). Furthermore, band-pass filtering was not performed on the fNIRS time series before GC analysis since the model order would increase, which in turn would increase the number of spurious connections between the ROIs (Barnett and Seth 2011; Florin et al. 2010).

The GC analysis was based on a MVAR model. In contrast to dynamical causal modeling (DCM) (Garrido et al. 2007), GC does not require any a priori information about the connectivity in the network to be analyzed. The concept of GC, first defined by Granger (Granger 1969), states that if a prediction about a future state of time series

B is improved after incorporating the past knowledge of time series A, then time series A is causing time series B. In this study we used GC to quantify effective connectivity networks in the brain.

$$X_t = \sum_{j=1}^{p} a_1 X_{t-j} + \sum_{j=1}^{p} b_1 Z_{t-j} + \varepsilon_{1t} \qquad (1)$$

$$Z_t = \sum_{j=1}^{p} c_1 X_{t-j} + \sum_{j=1}^{p} d_1 Z_{t-j} + \varepsilon_{2t} \qquad (2)$$

Assume time series X and Z of length t shown in Eq. (1–2) with model order p. The model order describes the number of past values of the time series that are required to successfully predict the present value of the time series. The MVAR coefficients (a, b, c, d) define whether GC exists between the two time series, and also the extent of GC, if it exists. Let $\varepsilon_x(t)$ denote the prediction error (where $x = 1, 2$). In order to get a reliable prediction, the prediction error should be minimized. The covariance matrix for the prediction error is given by Eq. (3).

$$\sigma^2_{\mathrm{model}_1} = \begin{bmatrix} \mathrm{var}(\varepsilon_{1t}) & \mathrm{cov}(\varepsilon_{1t}, \varepsilon_{2t}) \\ \mathrm{cov}(\varepsilon_{2t}, \varepsilon_{1t}) & \mathrm{var}(\varepsilon_{2t}) \end{bmatrix} \qquad (3)$$

The same model but with the inclusion of one more time series Y as shown in Eqs. (4–6) and the corresponding

Fig. 2 The group mean source level EEG activation (coherence) maps shown on a MNI template axial slice representing the contralateral (*column 1*) sensorimotor cortex (SMC), (*column 2*) premotor cortex (PMC) and (*column 3*) dorsolateral prefrontal cortex (DLPFC) during the finger tapping (FT), simple finger sequence (SFS) and complex finger sequence (CFS) tasks of the right hand. The *color bar* indicates the minimum and maximum EEG source analysis EEG-EMG dynamical coherence values
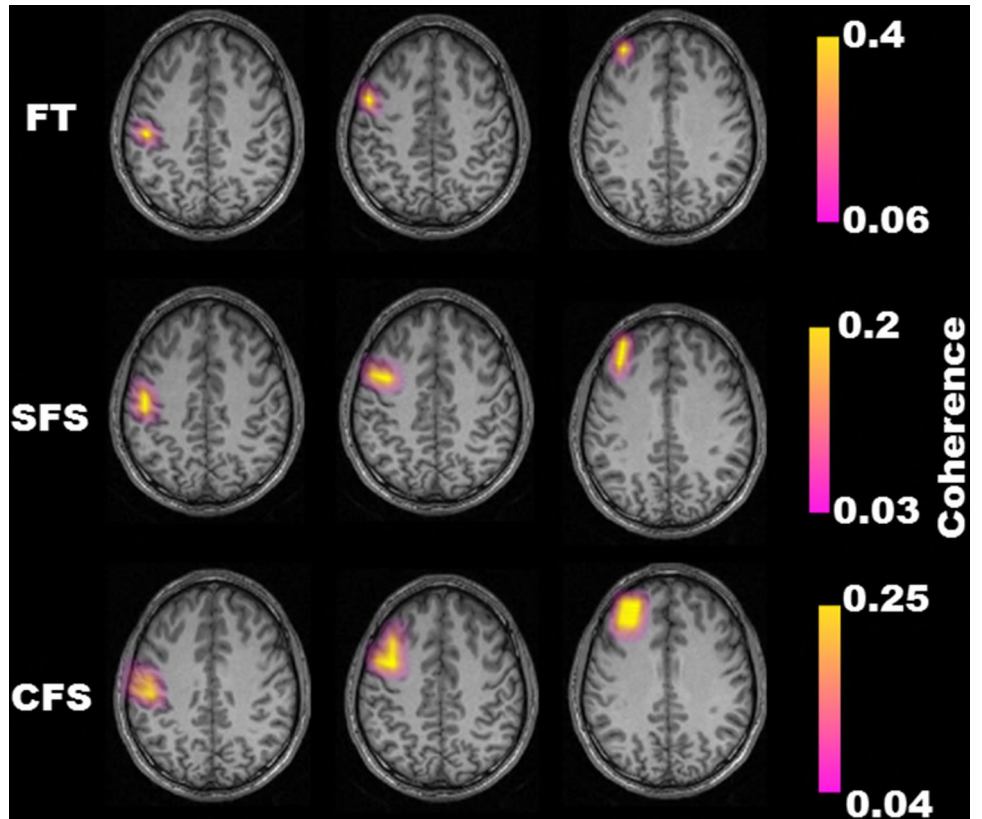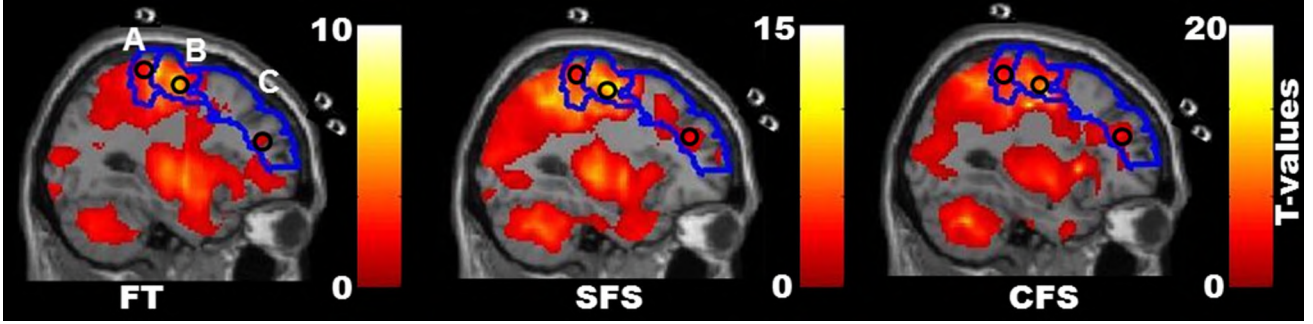
Fig. 3 The group mean fMRI (BOLD) activation maps shown on a MNI template sagittal slice representing the contralateral **a** sensori-motor cortex (SMC), **b** premotor cortex (PMC) and **c** dorsolateral prefrontal cortex (DLPFC) regions of interest (ROIs) during the finger tapping (FT), simple finger sequence (SFS), and complex finger sequence (CFS) tasks of the right hand. fNIRS fiducial markers are shown above the SMC (**a**). The *blue lines* indicate the three ROIs taken from an MNI anatomical automatic labeling atlas (AAL) and the three *black rings show* the 3-mm sphere around the maximum activated voxel of each ROI. The *color bar* indicates the minimum and maximum fMRI (*BOLD*) t-values (Color figure online)

covariance matrix is shown in Eq. (7). If this inclusion of Y actually reduces the prediction error of X, then Y is causing X, and the extent of GC can be quantified as the log ratio of the prediction error variance from both models by Eq. (8) (Seth 2010):

$$X_t = \sum_{j=1}^{p} a_2 X_{t-j} + \sum_{j=1}^{p} b_2 Y_{t-j} + \sum_{j=1}^{p} c_2 Z_{t-j} + \varepsilon_{3t} \quad (4)$$

$$Y_t = \sum_{j=1}^{p} d_2 X_{t-j} + \sum_{j=1}^{p} e_2 Y_{t-j} + \sum_{j=1}^{p} f_2 Z_{t-j} + \varepsilon_{4t} \quad (5)$$

$$Z_t = \sum_{j=1}^{p} g_2 X_{t-j} + \sum_{j=1}^{p} h_2 Y_{t-j} + \sum_{j=1}^{p} k_2 Z_{t-j} + \varepsilon_{5t} \quad (6)$$

$$\sigma^2_{model_2} = \begin{bmatrix} \text{var}(\varepsilon_{3t}) & \text{cov}(\varepsilon_{3t}, \varepsilon_{4t}) & \text{cov}(\varepsilon_{3t}, \varepsilon_{5t}) \\ \text{cov}(\varepsilon_{4t}, \varepsilon_{3t}) & \text{var}(\varepsilon_{4t}) & \text{cov}(\varepsilon_{4t}, \varepsilon_{5t}) \\ \text{cov}(\varepsilon_{5t}, \varepsilon_{3t}) & \text{cov}(\varepsilon_{5t}, \varepsilon_{4t}) & \text{var}(\varepsilon_{5t}) \end{bmatrix}$$

$$\quad (7)$$

$$F_{Y \to X|Z} = \log \left[\frac{\text{var}(\varepsilon_{1t})}{\text{var}(\varepsilon_{3t})} \right] \quad (8)$$

Before calculating GC, the model order p must be determined. The optimal model order must be an intermediate between a too simple (the model cannot capture important temporal dynamics) and a too complex model (model trap spurious causalities). Therefore, a compromise is needed between minimizing the prediction error variance and keeping the number of model parameters low enough. In this paper, we have chosen to minimize the Akaike Information Criterion (Akaike 1974) as an approach for estimating optimum model orders. For comparison of the GC values for all three modalities we have chosen the model order P = 5 for the fMRI, fNIRS and EEG

modalities after computing different model order for the three neuroimaging methods (fMRI: P = 4, fNIRS: P = 5 and EEG: P = 12) that produced no significant differences in connection strength by a link–link comparison of the connectivity values. Indeed, by using a non-parametric Kruskal–Wallis test followed by post hoc tests for independent samples, connection strength and the connectivity did not differ significantly between the three ROI's (SMC, PMC and DLPFC) for the three modalities. For application of GC, the GC connectivity analysis (GCCA) toolbox for (MATLAB R2013a, 8.1.0.604, The Mathworks Inc., MA, USA) was used (Seth 2010).

Due to the nonlinear relation between direct causality and time series data, the distribution of the MVAR coefficients is not well understood. This in turn indicates the need for a non-parametric significance test on the estimated GC amplitudes. Therefore, the time series subjected to GC were divided into smaller epochs and then appended in random order, such that by random shuffling of time series all the intrinsic GC was eliminated. GC was then calculated for this randomly shuffled EEG, fMRI and fNIRS time series; this was done 100 times and the mean result was used as our null hypothesis (Kamiński et al. 2001). Additionally, the time varying GC analysis was applied to 1-s data windows of the fNIRS and EEG data to estimate the time varying behavior of the connectivity over all the significant connections.

Statistical Analysis

The forward and backward GC values between the SMC, PMC, and DLPFC ROIs during each of the three finger movement tasks determined by EEG (scalp and source level), fNIRS (O₂Hb and HHb), and fMRI (BOLD) were tested using a non-parametric Kruskal–Wallis test followed by post hoc testing for independent samples (directionality connections

were: SMC → PMC, PMC → SMC, SMC → DLPFC, DLPFC → SMC, PMC → DLPFC, DLPFC → PMC). The forward and backward GC values between each modality (fNIRS, fMRI, EEG) were also tested using a non-parametric Kruskal–Wallis test followed by post hoc testing for independent samples. The Bonferroni correction was performed for the entire post hoc test that involved multiple comparisons. The significance level was set at $p < 0.05$.

Results

MNI Coordinates of the SMC, PMC, and DLPFC ROIs

The grand average activation maps from the EEG (source level) and fMRI (BOLD) are illustrated in Figs. 2 and 3, respectively (supplementary Fig. 2 shows the grand average activation time series and supplementary Table 1 shows the functional correlation between the EEG, fMRI and fNIRS modalities). The three finger movement tasks of the right hand were associated with an increase in activity in the contralateral SMC, PMC and DLPFC ROIs. The mean MNI co-ordinates and Euclidean distance between the EEG (source level) and fMRI (BOLD) in each of the three ROIs during the three finger movement tasks are

shown separately in Table 1. The MNI coordinates of all of the three identified ROIs (SMC, PMC and DLPFC) from the EEG and fMRI were statistically significant ($p = 0.003$) in a Monte Carlo random permutation test across all subjects for all the three motor tasks. The mean Euclidean distance between the maximum coherent voxel in the EEG source analysis and the fMRI maximum activated voxel in each of these three ROIs for the three tasks were within 3 mm (see Table 1). The mean estimated Euclidean distance between the scalp EEG electrodes and the maximum coherent voxel in the source level EEG ROIs (SMC: 25.3 ± 4.6 mm; PMC: 24.6 ± 3.9 mm; PFC: 26.5 ± 3.2 mm) and the maximum activated voxel in the fMRI ROIs (SMC: 24.7 ± 3.9 mm; PMC: 23.3 ± 4.1 mm; PFC: 25.9 ± 4.1 mm) was approximately 25 mm.

Effective Connectivity Determined by EEG, fMRI, and fNIRS

The forward and backward effective connectivity (GC values) between the SMC, PMC and DLPFC ROIs during the three motor tasks for each of the EEG, fMRI and fNIRS modalities are shown in Fig. 4 (and Fig. 5 shows the schematic in a representative template brain). In the case of scalp level EEG, GC analysis between the EEG electrodes representing the three ROIs (C3-SMC, FC3-PMC and F3-
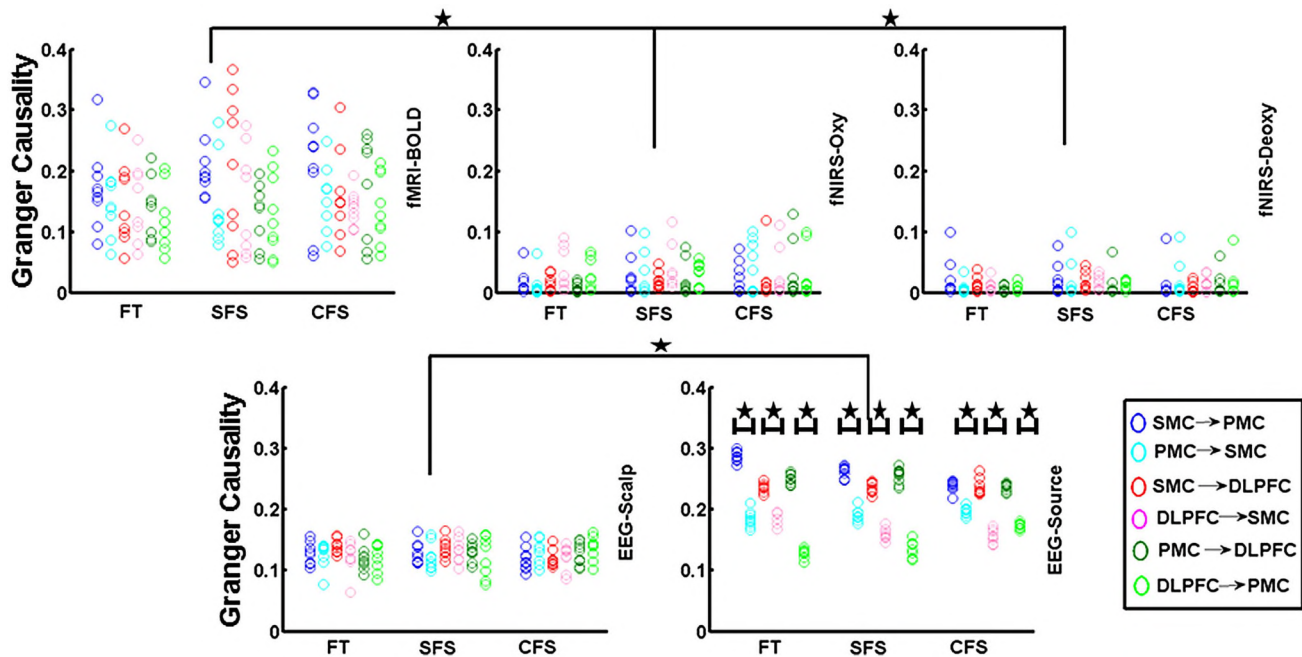

Fig. 4 Conditional Granger causality (GC) strength values of the direction of information flow between the sensorimotor cortex (SMC), premotor cortex (PMC) and dorsolateral prefrontal cortex (DLPFC) regions of interest (ROIs) measured by the EEG, fMRI and fNIRS modalities during the right hand finger tapping (FT), simple finger sequence (SFS), and complex finger sequence (CFS) tasks. The

Asterisk indicates a significant difference of GC values between the modalities fMRI and fNIRS in the first row. In the second row the *Asterisk* indicates a significant difference between the EEG-scalp and EEG source level analysis. Only in the EEG source level analysis there was a significant difference *Asterisk* between direct and the feedback direction
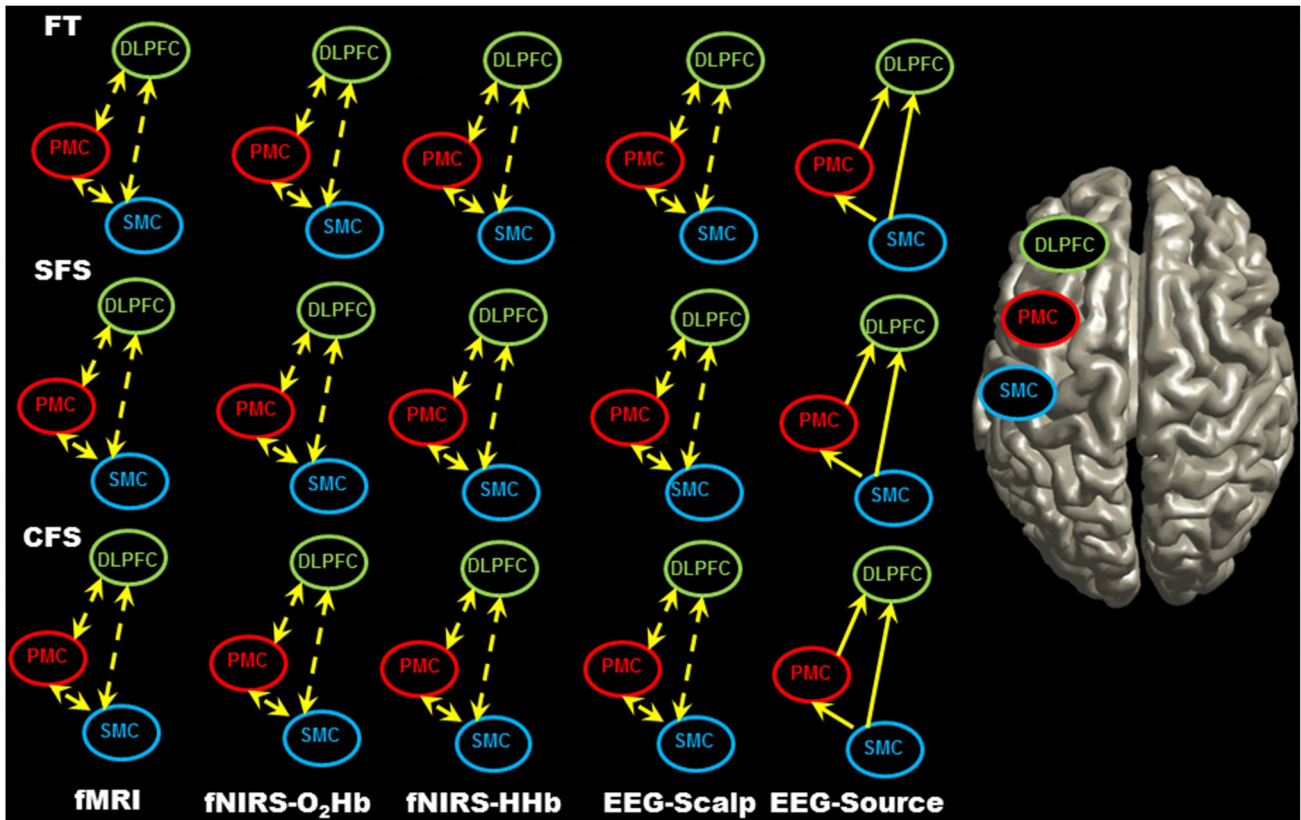
Fig. 5 Conditional Granger causality (GC) direction of information flow between the contralateral sensorimotor cortex (SMC), premotor cortex (PMC) and dorsolateral prefrontal cortex (DLPFC) regions of interest (ROIs) measured by the EEG, fMRI and fNIRS modalities during the finger tapping (FT), simple finger sequence (SFS), and complex finger sequence (CFS) tasks right hand. *Columns* indicate the different neuroimaging modalities, and *rows* indicate the different finger movement tasks. Only in the case of the EEG source level there was a significant difference between the direct and feedback direction. This is indicated in the figure with a *single arrow-head* and *yellow solid lines*

DLPFC) showed significant ($p = 0.023$; $p = 0.032$; $p = 0.021$, respectively) bi-directional connections (SMC $\leftrightarrow$ PMC, PMC $\leftrightarrow$ DLPFC, SMC $\leftrightarrow$ DLPFC) during all three motor tasks, with no significant difference between the forward and backward connections. In the case of source level EEG, there were also significant bi-directional connections ($p = 0.028$; $p = 0.025$; $p = 0.018$) between the three ROIs (SMC, PMC and DLPFC, respectively); however, there were also significant differences ($p = 0.018$; $p = 0.035$; $p = 0.028$) in the magnitude between the forward and backward connections, such that the forward connections from the SMC $\rightarrow$ PMC, PMC $\rightarrow$ DLPFC and SMC $\rightarrow$ DLPFC were significantly greater than the backward connections (PMC $\rightarrow$ SMC, DLPFC $\rightarrow$ SMC and DLPFC $\rightarrow$ PMC). In the case of fNIRS (O$_2$Hb and HHb) and fMRI (BOLD), there were also significant bi-directional connections ($p = 0.023$; $p = 0.018$; $p = 0.013$) between each of the three ROIs (SMC $\leftrightarrow$ PMC, PMC $\leftrightarrow$ DLPFC, SMC $\leftrightarrow$ DLPFC) over the three motor tasks, and although the forward connections were greater in magnitude compared to the backward direction, they were not significantly different ($p = 0.361$).

Additionally, time varying GC analysis for the fNIRS and EEG modalities were undertaken to test the influence of a higher temporal resolution (1 Hz) on the effective connectivity between the three ROIs (see supplementary Fig. 3). Similar to the GC results, the fNIRS and the EEG (scalp and source level) showed bi-directional connections between the ROIs, and only the source level EEG showed the forward connections were significantly greater than the backward connections.

The GC values for all three motor tasks were significantly higher for the source level EEG in comparison to scalp level EEG ($p = 0.004$), fMRI-BOLD ($p = 0.009$), fNIRS-O$_2$Hb ($p = 0.004$) and fNIRS-HHb ($p = 0.002$) (Fig. 4). Although the GC values between scalp level EEG and fMRI (BOLD) did not show any significant difference ($p = 0.457$), scalp level EEG GC values were significantly higher than fNIRS-O$_2$Hb ($p = 0.008$) and fNIRS-HHb

($p = 0.007$). The GC values were higher, but not significantly different ($p = 0.672$) for fNIRS-O_2Hb in comparison to the fNIRS-HHb. GC values for fMRI (BOLD) were significantly ($p = 0.003$) greater than fNIRS (O_2Hb and HHb). Even though we have compared the GC values between the modalities the interpretation of this result should be dealt with consideration. The results of the functional parcellation analyses were similar to the above results except the effective connectivity between SMC and DLPFC was significantly stronger. The results of these analyses are shown in supplementary Fig. 4.

Discussion

To the best of our knowledge, this is the first study to simultaneously apply EEG, fMRI and fNIRS neuroimaging modalities to independently determine using GC analysis the directional coupling (i.e., effective connectivity) between cortico-cortical sensorimotor networks (SMC, PMC and DLPFC) during finger movement tasks. A novel finding of this study was that the cortico-cortical effective connectivity determined by the fMRI, fNIRS and EEG modalities all showed a bi-directional information flow pattern between the SMC, PMC and DLPFC ROIs during the simple and complex finger movement tasks. However, the source level EEG provided the largest GC values and also showed a significantly greater forward than backward signal flow between the three ROIs.

Effective Connectivity Within Cortico-Cortical Networks

In the present study, we concentrated on three contralateral cortical ROIs (SMC, PMC, and DLPFC) to determine their effective connectivity during finger movement tasks of the right hand. We have studied the question of how well the electrophysiological (EEG) and hemodynamic (fMRI and fNIRS) neuroimaging modalities, measured in parallel, relate to each other in determining the information flow between the three cortical ROIs during performance of finger movement tasks. We found that the effective connectivity determined by GC analysis independently by the EEG (scalp and source), fMRI (BOLD) and fNIRS (O_2Hb and HHb) modalities shows a bidirectional flow of information between the SMC, PMC and DLPFC ROIs during performance of the finger movement tasks. These findings suggest that a bi-directional increase in information flow occurred between brain areas involved in activating finger movements (SMC), motor planning (PMC) and executive control (DLPFC). Our findings extend a previous fNIRS (Bajaj et al. 2014) and fMRI (Rehme et al. 2013) study that showed bi-directional effective connectivity between SMC

and PMC during performance of hand motor tasks. Our findings also agree with a study using transcranial magnetic stimulation (TMS) with event-related fMRI, which showed that the PMC and the SMC are strongly functionally connected and contribute significantly in performing a motor task (Bestmann et al. 2008). Furthermore, a paired pulse TMS paradigm showed temporally and spatially selective interactions between SMC and DLPFC that are both task and muscle specific (Hasan et al. 2013), which provides strong evidence for the effective connectivity between these ROIs shown in the present study. Furthermore, the connectivity between the human cortical motor systems have been validated earlier with in vivo cortical–cortical evoked potential and showed clearly the existing cortical–cortical connectivity (Matsumoto et al. 2007).

The directions of information flow for rhythmic movements in earlier studies have shown that the SMC plays a major role in directing voluntary motor tasks (Anwar et al. 2012; Kai et al. 2000; Zhang et al. 2010). A novel finding of the present study was that although scalp level EEG showed both forward and backward directions of information flow between ROIs with similar GC values, source level EEG, fNIRS (O_2Hb and HHb) and fMRI (BOLD) GC values were larger in the forward than backward direction (i.e., SMC → PMC, SMC → DLPFC, PMC → DLPFC), but this difference was only significant for source level EEG. The higher significance of the forward than backward directions of information flow between the three ROI's would suggest that the voluntary finger movements emerge from top-down processing that are less influenced by peripheral feedback which could lead to increasing the strength of backward connections as shown in previous studies (Muthuraman et al. 2012; Pollok et al. 2004, 2006). Even though, in this study we have compared the GC values between the modalities the interpretation of these results should be dealt with consideration has GC shows the effect and not the mechanism (Barrett and Barnett 2013). By using the three modalities simultaneously in one experiment we were able to show statistically that all three modalities show bi-directional information flow between the three ROI's. We tested the feasibility of combining the three functional neuroimaging modalities in one experiment and finally able to show how well the three functional neuroimaging modalities correspond to each other during an active motor task. However, for achieving a good spatial resolution and good temporal resolution the combination of fMRI and EEG could be used. However, the complete information of oxygenation and deoxygenation profile can be only obtained using fNIRS.

Methodological Considerations and Limitations

Functional connectivity is used to describe spatially separate ROIs that appear to be in close communication with

each other during performance of a task, based on coherence analysis of neuroimaging time series data. The rise of the concept of functional connectivity has led to the study of linked frequency responses measured by non-invasive neuroimaging modalities (Kinoshita et al. 2010). The choice of methods for functional connectivity is still a matter of intense research and debate (Stephan and Friston 2010). Recent advances in neuroimaging signal analyses have enabled researchers to estimate effective connectivity between cortical ROIs involved in task performance (Friston et al. 2003). Various methods for effective connectivity estimation between simultaneously recorded time series signals exist. The majority of these methods are based on the parameters of predictive models fitted to the data. Methods like structural equation modeling (SEM) (Büchel and Friston 1997) and dynamic causal modeling (DCM) (Friston et al. 2003) have traditionally been applied to the fMRI modality. One limiting factor for these two methods is the fact that their results are always based on some a priori assumptions about the anatomical networks. GC-estimating methods like partial directed coherence (PDC) (Baccalá and Sameshima 2001), directed transfer function (DTF) (Kaminski and Blinowska 1991), modified directed transfer function (dDTF), generalized partial directed coherence (gPDC) (Baccalá et al. 2007) and renormalized partial directed coherence (rPDC) (Schelter et al. 2009) are all parametric measures of effective connectivity that don't require a priori anatomical knowledge. Furthermore, they infer the effective connectivity in the frequency domain and hence are useful in analyzing brain networks corresponding to certain frequencies of interest.

The GC analysis in the time domain has been widely used in neurological signal processing for the estimation of effective connectivity. Recent literature has compared the performance of GC measures for a variety of signal scenarios like fMRI and results show that the GC is a quite robust measure of effective connectivity in the case of the variable hemodynamic response function (HRF). Furthermore, GC is invariant to the convolution of the neural signal with the HRF (Seth et al. 2013). Moreover, GC is shown to be invariant under quite a few classes of filtering operations and not down sampling (Barnett and Seth 2011; Seth et al. 2013). Finally, it has also been shown that GC provides reliable results for many different HRF systems including 'time-to-peak' confound (Seth et al. 2013; Wen et al. 2013). In the present study, due to the limited time resolution of fMRI (0.4 Hz) compared to the fNIRS (10 Hz) and EEG (1000 Hz), we considered that using GC in the time domain to be the optimal method to infer the directionality information between the time series (Seth 2010) of the three cortical ROIs measured by the fMRI, fNIRS and EEG modalities. However, there are some issues that need to be considered.

Firstly, it should be noted that the full spatial resolution of the fMRI modality was not utilized in this study by selecting only 3 ROIs, but we chose a limited number of ROIs to make comparisons between the lower spatial resolutions of the EEG and fNIRS modalities. Since we did not utilize the full time resolution of the fNIRS and EEG for the GC analysis, we looked into by estimating the time varying GC analysis of the EEG and fNIRS modalities using their full time resolutions (see supplementary Fig. 3). The results for this analysis showed similar GC values to the present results, which suggests that the greater GC values attained by the source level EEG is not merely due to the improved temporal resolution. Additionally the greater spatial accuracy of source level EEG provides a better estimate of the source of activation, which was evident from the close correspondence of the location of the maximum activated voxel between the source level EEG and fMRI (see Table 1).

Secondly, there could be an issue on the selection of the ROIs for the fMRI modality using a sphere around a seed voxel parcellation method. Some studies have reported different results based on different parcellation techniques, which raises a question mark on the appropriateness of different parcellation techniques (Shirer et al. 2012; Sohn et al. 2015; van den Heuvel and Sporns 2011; Wang et al. 2009). Two parameters contribute to the inter-subject anatomical variability, first brains vary in their folding patterns and second brains vary in terms of location of the cytoarchitectonic zones, which plausibly correspond to the function (Nieto-Castañón and Fedorenko 2012). In order to overcome these two problems, we used a technique based on a "localizer" or ROI, which has been used extensively in the literature, where we determined a subject-specific ROI (Nieto-Castañón and Fedorenko 2012). After estimating the local ROI with maximum activation, we validated further the position of that ROI in the brain using its MNI coordinates and using a brain atlas from SPM8. A sphere radius of 3 mm was used in this study to restrict the extracted signal clearly to the selected brain regions (Zhang et al. 2010). In order to check the correspondence of our results to a parcellation, fMRI data was parcelled using an anatomical template namely Automated Anatomic Labelling (AAL) atlas and then the fMRI-BOLD signals were extracted from the three ROIS (SMC, PMC and DLPFC) and the GC analyses were repeated to see the effective connectivity (see supplementary Fig. 4). The results were similar to our previous results except the effective connectivity between SMC and DLPFC that was significantly stronger. We did not consider this parcellation method for this study since the main focus of the study was to use the EMG as EEG reference and identify the coherent network of sources for each motor task.

Thirdly, since down sampling the data could lead to false results, we checked for consistency by reducing the

number of time points progressively and checked the significance threshold for the three finger movement tasks separately for our fMRI data. The significance threshold did not vary significantly for the three tasks FT ($p = 0.57$), SFS ($p = 0.47$) and CFS ($p = 0.39$). Thus the surrogate method used was considered valid in the present study.

Fourthly, the EEG-EMG coherence was the basis for selecting the peak frequency in the band (2–5 Hz) in this study for the subsequent source and effective connectivity analyses. In order to understand the network involved during the motor tasks at this band (2–5 Hz), we have undertaken the band-limited EEG analyses and showed a different network of sources for the three different motor tasks namely the posterior parietal cortex (PPC), medial frontal cortex (MFC) and prefrontal cortex (PFC). The effective connectivity between the sources was then analyzed using Granger causality and the results are shown in supplementary Fig. 5.

Finally, the scalp level EEG method suffers from noise and volume conduction effects (Schlogl and Supp 2006), and this can be circumvented by looking at the connectivity measures using source level EEG (Astolfi et al. 2009; Hassan et al. 2014). In particular for EEG signals, a linear AR model may lead to wrong estimations of GC. Although nonlinear measures like mutual information might be preferred when studying broadband EEG signals with nonlinearities, linear methods are still preferred as they offer a rapid and easy characterization of functionality (Astolfi and Babiloni 2007). A recent study applied DTF and PDC (both are based on GC measures) on nonlinear data and demonstrated that by using the sufficiently high model order, nonlinear interactions within the data were captured as well by these linear connectivity measures (Astolfi and Babiloni 2007; Seth et al. 2015). We have previously tested a nonlinear version of GC by using the time domain partial directed coherence which uses the dual extended Kalman filter in the time domain (Anwar et al. 2013, 2014). We tested this nonlinear GC method on the EEG signals and compared the differences to the present study linear version GC results. The results for the effective connectivity analyses on the scalp EEG and on the source EEG signals showed no differences between the linear and non-linear GC methods in the significant connections between the three ROIs. The application of non-linear connectivity analyses was also tested using the time domain partial directed coherence (TPDC) method which uses the dual extended Kalman filter in the time domain (Anwar et al. 2013, 2014). We have compared the strength of each link between ROIs by a link–link comparison with a non-parametric Kruskal–Wallis test. The results for the scalp level EEG comparing the nonlinear TPDC and linear GC revealed no significant

difference for the three tasks. Similarly on the EEG source level the analyses did not reveal any significant difference for the three tasks. Altogether, these findings confirm that the non-linear connectivity analyses were not different to the results from the linear GC method in the context of our study. These empirical findings indicate that a nonlinear GC method approach was not superior to the linear GC one in assessing causality in cortical activity variability series recorded from healthy subjects. This confirms that Granger causality based on a linear model is able to detect and quantify changes in coupling strength and direction of activation between different cortical regions (Astolfi and Babiloni 2007; Seth et al. 2015). In pathological population, where the contribution of nonlinearities might be more evident, the advantage of using a nonlinear GC method might become a tool to quantify more constantly than linear GC approaches causality in cortical regions. In addition, overall, we suggest that no single method can be recognized as the best in all circumstances, and each of the methods has its domain of best applicability.

Conclusion

This simultaneous fMRI, fNIRS and EEG study has shown for the first time that a bi-directional effective connectivity exists within a cortico-cortical sensorimotor network (SMC, PMC and DLPFC) during finger movement tasks of different complexity. However, since information flow data acquired with source level EEG showed the largest GC amplitude values compared to scalp EEG, fNIRS and fMRI, we consider that source level EEG provides the strongest means to characterize the directionality of neural communication within cortico-cortical sensorimotor networks; however, fMRI or fNIRS could be used to guide the source localization. The source level EEG changes in functional activation and effective connectivity analysis to different neurological conditions (Japaridze et al. 2013; Muthuraman et al. 2012) can be employed in the future as a diagnostic tool for following the progress to clinical studies. Since fNIRS is more easy to use with fewer constraints than fMRI, it is an attractive alternative to fMRI in particular for providing reasonable spatial resolution for bedside multimodal fNIRS-EEG measurements.

publication. We would also like to thank Marco Dat for assisting with the experimental setup.

References

Abler B, Roebroeck A, Goebel R, Höse A, Schönfeldt-Lecuona C, Hole G, Walter H (2006) Investigating directed influences between activated brain areas in a motor-response task using fMRI. Magn Reson Imaging 24:181–185. doi:10.1016/j.mri.2005.10.022

Akaike H (1974) A new look at the statistical model identification. IEEE Trans Autom Control 19:716–723. doi:10.1109/TAC.1974.1100705

Anwar AR et al (2012) Directionality analysis on functional magnetic resonance imaging during motor task using Granger Causality. In: Engineering in medicine and biology society (EMBC), 2012 Annual international conference of the IEEE, Aug. 28 2012–Sep 1 2012, pp 2287–2290. doi:10.1109/EMBC.2012.6346419

Allen PJ, Polizzi G, Krakow K, Fish DR, Lemieux L (1998) Identification of EEG events in the MR scanner: the problem of pulse artifact and a method for its subtraction. NeuroImage 8:229–239. doi:10.1006/nimg.1998.0361

Allen PJ, Josephs O, Turner R (2000) A Method for Removing Imaging Artifact from Continuous EEG Recorded during. Funct MRI NeuroImage 12:230–239. doi:10.1006/nimg.2000.0599

Amjad AM, Halliday DM, Rosenberg JR, Conway BA (1997) An extended difference of coherence test for comparing and combining several independent coherence estimates: theory and application to the study of motor units and physiological tremor. J Neurosci Methods 73:69–79

Andres FG, Gerloff C (1999) Coherence of sequential movements and motor learning. J Clin Neurophysiol 16:520–527

Anwar AR et al (2013) Comparison of causality analysis on simultaneously measured fMRI and NIRS signals during motor tasks. Conf Proc IEEE Eng Med Biol Soc 2013:2628–2631. doi:10.1109/embc.2013.6610079

Anwar AR et al (2014) Multi-modal causality analysis of eyes-open and eyes-closed data from simultaneously recorded EEG and MEG. Conf Proc IEEE Eng Med Biol Soc 2014:2825–2828. doi:10.1109/embc.2014.6944211

Astolfi L, Babiloni F (2007) Estimation of cortical connectivity in humans: advanced signal processing techniques. Estimation of cortical connectivity in humans: advanced signal processing techniques. Morgan & Claypool, San Rafael. doi:10.2200/S00094ED1V01Y200708BME013

Astolfi L, Cichocki A, Babiloni F (2009) NeuroMath: advanced methods for the estimation of human brain activity and connectivity. Comput Intell Neurosci. doi:10.1155/2009/275638

Attwell D, Iadecola C (2002) The neural basis of functional brain imaging signals. Trends Neurosci 25:621–625. doi:10.1016/S0166-2236(02)02264-6

Baccalá LA, Sameshima K (2001) Partial directed coherence: a new concept in neural structure determination. Biol Cybern 84:463–474. doi:10.1007/PL00007990

Baccalá LA, Sameshima K, Takahashi DY (2007) Generalized partial directed coherence. In: 2007 15th International conference on digital signal processing, 1–4 July 2007, pp 163–166. doi:10.1109/ICDSP.2007.4288544

Bajaj S, Drake D, Butler AJ, Dhamala M (2014) Oscillatory motor network activity during rest and movement: an fNIRS study. Front Syst Neurosci 8:13. doi:10.3389/fnsys.2014.00013

Barnett L, Seth AK (2011) Behaviour of Granger causality under filtering: theoretical invariance and practical application. J Neurosci Methods 201:404–419. doi:10.1016/j.jneumeth.2011.08.010

Barrett AB, Barnett L (2013) Granger causality is designed to measure effect, not mechanism. Front Neuroinformatics 7:6. doi:10.3389/fninf.2013.00006

Bestmann S et al (2008) Dorsal premotor cortex exerts state-dependent causal influences on activity in contralateral primary motor and dorsal premotor cortex. Cereb Cortex 18:1281–1291. doi:10.1093/cercor/bhm159

Biswal B, Yetkin FZ, Haughton VM, Hyde JS (1995) Functional connectivity in the motor cortex of resting human brain using echo-planar MRI. Magn Reson Med 34:537–541

Blinowska KJ, Malinowski M (1991) Non-linear and linear forecasting of the EEG time series. Biol Cybern 66:159–165

Büchel C, Friston KJ (1997) Modulation of connectivity in visual pathways by attention: cortical interactions evaluated with structural equation modelling and fMRI. Cereb Cortex 7:768–778. doi:10.1093/cercor/7.8.768

Cohen D (1968) Magnetoencephalography: evidence of magnetic fields produced by alpha-rhythm currents. Science (New York, NY) 161:784–786

Engel AK, Fries P, Singer W (2001) Dynamic predictions: oscillations and synchrony in top-down processing. Nat Rev Neurosci 2:704–716

Ewald A, Marzetti L, Zappasodi F, Meinecke FC, Nolte G (2012) Estimating true brain connectivity from EEG/MEG data invariant to linear and static transformations in sensor space. Neuroimage 60:476–488. doi:10.1016/j.neuroimage.2011.11.084

Ferrari M, Quaresima V (2012) A brief review on the history of human functional near-infrared spectroscopy (fNIRS) development and fields of application. Neuroimage 63:921–935

Florin E, Gross J, Pfeifer J, Fink GR, Timmermann L (2010) The effect of filtering on Granger causality based multivariate causality measures. NeuroImage 50:577–588

Friston KJ, Harrison L, Penny W (2003) Dynamic causal modelling. NeuroImage 19:1273–1302. doi:10.1016/S1053-8119(03)00202-7

Fuchs M, Kastner J, Wagner M, Hawes S, Ebersole JS (2002) A standardized boundary element method volume conductor model. Clin Neurophysiol 113:702–712

Garrido MI, Kilner JM, Kiebel SJ, Stephan KE, Friston KJ (2007) Dynamic causal modelling of evoked potentials: a reproducibility study. Neuroimage 36:571–580. doi:10.1016/j.neuroimage.2007.03.014

Govindan RB, Raethjen J, Kopper F, Claussen JC, Deuschl G (2005) Estimation of time delay by coherence analysis. Phys A 350:277–295

Granger CWJ (1969) Investigating causal relations by econometric models and cross-spectral methods. Econometrica 37:424–438. doi:10.2307/1912791

Gratton G, Coles MGH, Donchin E (1983) A new method for off-line removal of ocular artifact. Electroencephalogr Clin Neurophysiol 55:468–484

Gross J, Kujala J, Hamalainen M, Timmermann L, Schnitzler A, Salmelin R (2001) Dynamic imaging of coherent sources: Studying neural interactions in the human brain. Proc Natl Acad Sci USA 98:694–699

Halliday DM, Rosenberg JR, Amjad AM, Breeze P, Conway BA, Farmer SF (1995) A framework for the analysis of mixed time series/point process data–theory and application to the study of

physiological tremor, single motor unit discharges and electromyograms. Prog Biophys Mol Biol 64:237–278

Hasan A, Galea JM, Casula EP, Falkai P, Bestmann S, Rothwell JC (2013) Muscle and timing-specific functional connectivity between the dorsolateral prefrontal cortex and the primary motor cortex. J Cogn Neurosci 25:558–570. doi:10.1162/jocn_a_00338

Hassan M, Dufor O, Merlet I, Berrou C, Wendling F (2014) EEG source connectivity analysis: from dense array recordings to brain networks. PloS One 9:e105041. doi:10.1371/journal.pone.0105041

Hwang K, Velanova K, Luna B (2010) Strengthening of top-down frontal cognitive control networks underlying the development of inhibitory control: a functional magnetic resonance imaging effective connectivity study. J Neurosci 30:15535–15545. doi:10.1523/JNEUROSCI.2825-10.2010

Im C-H, Jung Y-J, Lee S, Koh D, Kim D-W, Kim B-M (2010) Estimation of directional coupling between cortical areas using Near-Infrared Spectroscopy (NIRS). Opt Express 18:5730–5739

Japaridze N et al (2013) Neuronal networks in west syndrome as revealed by source analysis and renormalized partial directed coherence. Brain Topogr 26:157–170. doi:10.1007/s10548-012-0245-y

Journee HL (2007) Demodulation of amplitude modulated noise: a mathematical evaluation of a demodulator for pathological tremor. In: EMG's IEEE transactions on biomedical engineering, pp 304–308

Kai L, Karsten S, Jon Shah N, Lutz J (2000) Tapping movements according to regular and irregular visual timing signals investigated with fMRI. Neuro Rep 11:1301–1306

Kaminski MJ, Blinowska KJ (1991) A new method of the description of the information flow in the brain structures. Biol Cybern 65:203–210

Kamiński M, Ding M, Truccolo WA, Bressler SL (2001) Evaluating causal relations in neural systems: Granger causality, directed transfer function and statistical assessment of significance. Biol Cybern 85:145–157. doi:10.1007/s004220000235

Kikuchi T, Miller JM, Schneck N, Oquendo MA, Mann JJ, Parsey RV, Keilp JG (2012) Neural responses to incongruency in a blocked-trial Stroop fMRI task in major depressive disorder. J Affect Disord 143:241–247. doi:10.1016/j.jad.2012.05.016

Kinoshita M et al (2010) How does voluntary movement stop resting tremor? Clin Neurophysiol 121:983–985

Korzeniewska A, Manczak M, Kaminski M, Blinowska KJ, Kasicki S (2003) Determination of information flow direction among brain structures by a modified directed transfer function (dDTF) method. J Neurosci Methods 125:195–207

Leff DR, Orihuela-Espina F, Elwell CE, Athanasiou T, Delpy DT, Darzi AW, Yang GZ (2011) Assessment of the cerebral cortex during motor task behaviours in adults: a systematic review of functional near infrared spectroscopy (fNIRS) studies. Neuroimage 54:2922–2936

Leuchter AF, Newton TF, Cook IA, Walter DO, Rosenberg-Thompson S, Lachenbruch PA (1992) Changes in brain functional connectivity in Alzheimer-type and multi-infarct dementia. Brain 115(Pt 5):1543–1561

Matsumoto R, Nair DR, LaPresto E, Bingaman W, Shibasaki H, Luders HO (2007) Functional connectivity in human cortical motor system: a cortico-cortical evoked potential study. Brain 130:181–197. doi:10.1093/brain/awl257

Michels L et al (2013) Developmental changes of functional and directed resting-state connectivities associated with neuronal oscillations in EEG. NeuroImage 81:231–242. doi:10.1016/j.neuroimage.2013.04.030

Muthalib M et al (2013) Multimodal integration of fNIRS, fMRI and EEG neuroimaging. Clin Neurophysiol 124:2060–2062. doi:10.1016/j.clinph.2013.03.018

Muthuraman M, Heute U, Arning K, Anwar AR, Elble R, Deuschl G, Raethjen J (2012) Oscillating central motor networks in pathological tremors and voluntary movements. What makes the difference? NeuroImage 60:1331–1339

Nedelko V et al (2010) Age-independent activation in areas of the mirror neuron system during action observation and action imagery. A fMRI study. Restor Neurol Neurosci 28:737–747

Niedermeyer E, da Silva FHL (2005) Electroencephalography: basic principles, clinical applications, and related fields. Lippincott Williams & Wilkins, Philadelphia

Nieto-Castañón A, Fedorenko E (2012) Subject-specific functional localizers increase sensitivity and functional resolution of multi-subject analyses. NeuroImage 63:1646–1669. doi:10.1016/j.neuroimage.2012.06.065

Nikouline VV, Linkenkaer-Hansen K, Huttunen J, Ilmoniemi RJ (2001) Interhemispheric phase synchrony and amplitude correlation of spontaneous beta oscillations in human subjects: a magnetoencephalographic study. NeuroReport 12:2487–2491

Oldfield RC (1971) The assessment and analysis of handedness: the Edinburgh inventory. Neuropsychologia 9:97–113

Oostenveld R, Fries P, Maris E, Schoffelen J-M (2010) FieldTrip: open source software for advanced analysis of MEG, EEG, and invasive electrophysiological data. Comput Intell Neurosci. doi:10.1155/2011/156869

Pollok B, Gross J, Dirks M, Timmermann L, Schnitzler A (2004) The cerebral oscillatory network of voluntary tremor. J Physiol 554:871–878

Pollok B, Gross J, Schnitzler A (2006) How the brain controls repetitive finger movements. J Physiol-Paris 99:8–13. doi:10.1016/j.jphysparis.2005.06.002

Rehme AK, Eickhoff SB, Grefkes C (2013) State-dependent differences between functional and effective connectivity of the human cortical motor system. Neuroimage 67:237–246. doi:10.1016/j.neuroimage.2012.11.027

Rosenberg JR, Amjad AM, Breeze P, Brillinger DR, Halliday DM (1989) The Fourier approach to the identification of functional coupling between neuronal spike trains. Prog Biophys Mol Biol 53:1–31

Schelter B et al (2006) Testing for directed influences among neural signals using partial directed coherence. J Neurosci Methods 152:210–219. doi:10.1016/j.jneumeth.2005.09.001

Schelter B, Timmer J, Eichler M (2009) Assessing the strength of directed influences among neural signals using renormalized partial directed coherence. J Neurosci Methods 179:121–130. doi:10.1016/j.jneumeth.2009.01.006

Schlogl A, Supp G (2006) Analyzing event-related EEG data with multivariate autoregressive parameters. Prog Brain Res 159:135–147. doi:10.1016/s0079-6123(06)59009-0

Schnitzler A, Gross J (2005) Functional connectivity analysis in magnetoencephalography. Int Rev Neurobiol 68:173–195. doi:10.1016/s0074-7742(05)68007-5

Sekihara K, Scholz B (1996) Generalized Wiener estimation of three-dimensional current distribution from biomagnetic measurements. IEEE Trans Biomed Eng 43:281–291

Seth AK (2010) A MATLAB toolbox for Granger causal connectivity analysis. J Neurosci Methods 186:262–273. doi:10.1016/j.jneumeth.2009.11.020

Seth AK, Chorley P, Barnett LC (2013) Granger causality analysis of fMRI BOLD signals is invariant to hemodynamic convolution but not downsampling. NeuroImage 65:540–555. doi:10.1016/j.neuroimage.2012.09.049

Seth AK, Barrett AB, Barnett L (2015) Granger causality analysis in neuroscience and neuroimaging. J Neurosci 35:3293–3297. doi:10.1523/jneurosci.4399-14.2015

Shibasaki H (2008) Human brain mapping: hemodynamic response and electrophysiology. Clin Neurophysiol 119:731–743

Shirer WR, Ryali S, Rykhlevskaia E, Menon V, Greicius MD (2012) Decoding subject-driven cognitive states with whole-brain connectivity patterns. Cerebral cortex (New York, NY) 22:158–165. doi:10.1093/cercor/bhr099

Sohn WS, Yoo K, Lee YB, Seo SW, Na DL, Jeong Y (2015) Influence of ROI selection on resting state functional connectivity: an individualized approach for resting state fMRI analysis. Front Neurosci 9:280. doi:10.3389/fnins.2015.00280

Stephan KE, Friston KJ (2010) Analyzing effective connectivity with functional magnetic resonance imaging. Wiley Interdiscip Rev 1:446–459. doi:10.1002/wcs.58

van den Heuvel MP, Sporns O (2011) Rich-club organization of the human connectome. J Neurosci 31:15775–15786. doi:10.1523/jneurosci.3539-11.2011

Van Veen BD, Van Drongelen W, Yuchtman M, Suzuki A (2002) Localization of brain electrical activity via linearly constrained minimum variance spatial filtering. IEEE Trans Biomed Eng 44:867–880

Wang J et al (2009) Parcellation-dependent small-world brain functional networks: a resting-state fMRI study. Hum Brain Mapp 30:1511–1523. doi:10.1002/hbm.20623

Wen X, Yao L, Liu Y, Ding M (2012) Causal interactions in attention networks predict behavioral performance. J Neurosci 32:1284–1292. doi:10.1523/JNEUROSCI.2817-11.2012

Wen X, Rangarajan G, Ding M (2013) Is Granger causality a viable technique for analyzing fMRI data? PloS One 8:e67428. doi:10.1371/journal.pone.0067428

Witt ST, Laird AR, Meyerand ME (2008) Functional neuroimaging correlates of finger-tapping task variations: an ALE meta-analysis. Neuroimage 42:343–356

Wu T, Hallett M (2005) The influence of normal human ageing on automatic movements. J Physiol 562:605–615. doi:10.1113/jphysiol.2004.076042

Xiong J, Parsons LM, Gao JH, Fox PT (1999) Interregional connectivity to primary motor cortex revealed using MRI resting state images. Hum Brain Mapp 8:151–156

Yuan Z (2013) Combining independent component analysis and Granger causality to investigate brain network dynamics with fNIRS measurements. Biomed Opt Express 4:2629–2643. doi:10.1364/boe.4.002629

Zhang L, Zhong G, Wu Y, Vangel M, Jiang B, Kong J (2010) Using granger-geweke causality model to evaluate the effective connecitivty of primary motor cortex, supplementary motor area and cerebellum. J Biomed Sci Eng 3:848–860